Title

Engineering Photocrosslinkable Bicomponent Hydrogel Constructs for Creating 3D Vascularized Bone.

Journal

Advanced healthcare materials, 6(10)

ISSN

2192-2640

Authors

Kazemzadeh-Narbat, Mehdi
Rouwkema, Jeroen
Annabi, Nasim
et al.

Publication Date

2017-05-01

DOI

10.1002/adhm.201601122

Peer reviewed

Engineering Photocrosslinkable Bicomponent Hydrogel Constructs for Creating 3D Vascularized Bone

Mehdi Kazemzadeh-Narbat, Jeroen Rouwkema, Nasim Annabi, Hao Cheng, Masoumeh Ghaderi, Byung-Hyun Cha, Mansi Aparnathi, Akbar Khalilpour, Batzaya Byambaa, Esmaiel Jabbari, Ali Tamayol,* and Ali Khademhosseini**

Engineering bone tissue requires the generation of a highly organized vasculature. Cellular behavior is affected by the respective niche. Directing cellular behavior and differentiation for creating mineralized regions surrounded by vasculature can be achieved by controlling the pattern of osteogenic and angiogenic niches. This manuscript reports on engineering vascularized bone tissues by incorporating osteogenic and angiogenic cell-laden niches in a photocrosslinkable hydrogel construct. Two-step photolithography process is used to control the stiffness of the hydrogel and distribution of cells in the patterned hydrogel. In addition, osteoinductive nanoparticles are utilized to induce osteogenesis. The size of microfabricated constructs has a pronounced effect on cellular organization and function. It is shown that the simultaneous presence of both osteogenic and angiogenic niches in one construct results in formation of mineralized regions surrounded by organized vasculature. In addition, the presence of angiogenic niche improves bone formation. This approach can be used for engineered constructs that can be used for treatment of bone defects.

1. Introduction

Even though bone tissue has a remarkable regenerative capacity, large bone defects are often unable to fully heal on their own partially due to the destruction of the local vascular network.[1,2] Traditional approaches for treatment of large bone defects include autologous bone transplantation and cancellous bone allografts.[3] Allografts carry the risk of immune rejection.[4–7] Autologous bone grafts, particularly vascularized grafts of the fibula and iliac crest, are effective in the treatment of large bone defects since they provide both an osteogenic environment and a vascular network.[8] However, their shortcomings remain an obstacle, for example, harvesting autografts is time consuming, expensive, and associated with infection,

Dr. M. Kazemzadeh-Narbat, Dr. J. Rouwkema, Dr. N. Annabi, Dr. H. Cheng, Dr. M. Ghaderi, Dr. B.-H. Cha, Dr. M. Aparnathi, Dr. A. Khalilpour, Dr. B. Batzaya, Dr. A. Tamayol, Prof. A. Khademhosseini
Biomaterials Innovation Research Center
Department of Medicine
Brigham and Women's Hospital
Harvard Medical School
Boston, MA 02139, USA
E-mail: n.annabi@neu.edu; atamayol@partners.org; alik@bwh.harvard.edu

Dr. M. Kazemzadeh-Narbat, Dr. J. Rouwkema, Dr. N. Annabi, Dr. H. Cheng, Dr. M. Ghaderi, Dr. B.-H. Cha, Dr. M. Aparnathi, Dr. A. Khalilpour, Dr. B. Batzaya, Dr. A. Tamayol, Prof. A. Khademhosseini
Harvard-MIT Division of Health Sciences and Technology
Massachusetts Institute of Technology
Cambridge, MA 02139, USA

Prof. J. Rouwkema
Department of Biomechanical Engineering
MIRA Institute for Biomedical Technology and Technical Medicine
University of Twente
7522NB Enschede, The Netherlands

Dr. N. Annabi, Dr. A. Tamayol, Prof. A. Khademhosseini
Wyss Institute for Biologically Inspired Engineering
Harvard University
Boston, MA 02115, USA

Prof. N. Annabi
Department of Chemical Engineering
Northeastern University
Boston, MA 02115-5000, USA

Prof. E. Jabbari
Biomimetic Materials and Tissue Engineering Laboratories
Department of Chemical Engineering
University of South Carolina
Columbia, SC 29208, USA

Prof. A. Khademhosseini
Department of Physics
King Abdulaziz University
Jeddah 21569, Saudi Arabia

Prof. A. Khademhosseini
Department of Bioindustrial Technologies
College of Animal Bioscience and Technology
Konkuk University
Seoul 05029, Republic of Korea

DOI: 10.1002/adhm.201601122

pain, and hematoma and major microsurgical operative procedures are required for transplantation of vascular autografts.[3,9] Thus, a new paradigm is required for treatment of large bone defects.

Tissue engineering strategies provide an alternative solution for the treatment of large bone defects. According to preclinical reports, cell-based tissue-engineered constructs are capable of inducing more bone formation compared to acellular constructs.[10] By combining patient-derived cells with biomaterial scaffolds and/or extracellular matrix (ECM) analogues, large volumes of tissue analogues can be prepared.[11,12] However, these strategies have not been successful in accommodating proper vasculature to compensate slow invasion/perfusion of the host vasculature into the scaffold.[1,6,11,13] Poor vascularization results in ischemia and subsequently poor cell survival and function within days of implantation.[14,15] Thus, engineering strategies to enhance vascularization has been the focus of several studies.[12,15–17] The strategies followed in these studies can be broadly divided into two groups: (1) engineering prevascularized constructs so that they can develop angiogenic cues through their encapsulated cells and (2) employing biological processes for self-formation of effective vasculature.[18,19] However, there are limitations to either of these approaches, such as poor resolution of fabricated vascular patterns and inability to direct the organization of the formed structures.[1,4] A promising approach to address these challenges is to engineer tissue constructs with predefined spatial distribution of angiogenic cues to direct the architecture of the formed vasculature.[18] Even though studies on prevascularized bone tissue engineering have been successful in showing the potential of this approach, parallel optimization of both osteogenesis and angiogenesis is challenging.[10,20,21] The two tissue structures require different microenvironments with regards to biomaterial chemistry, matrix mechanical properties, and the availability of morphogens and growth factors.[6,22] This is unattainable using standard tissue engineering approaches, where all cells are mixed and therefore experience the same external cues. A methodology that is capable of patterning local environments within a single tissue construct would allow for the optimization of conditions for both tissues, while still benefiting from the interactions between different cell types. Approaches where growth factors are patterned within hydrogels in order to achieve vascularized bone tissue have for instance been investigated.[23,24] Coupling osteogenic and angiogenic cues in a scaffold can potentially form an early vascular network by encapsulated cells preventing an ischemic environment to sustain cellular viability in nonhealing defects. An engineered biomaterial for this purpose should be able to mimic the natural bone ECM to promote bone healing as well as enhance 3D vascular network formation.[25]

Co-culture of osteogenic and endothelial cells has also shown that these systems result in an upregulation of both osteogenesis and angiogenesis, due to interactions between the two cell types.[10,20,21] These synergistic interactions between osteoblasts/osteogenic precursors and endothelial cells significantly improve the development of a vascular network that serves as a template for later ossification.[26] Apart from that, mesenchymal stem cells (MSCs), which are generally used as osteoprogenitor cells in these systems, can differentiate toward smooth muscle cells or pericytes and can stabilize the formed vascular structures when cultured in direct contact with endothelial cells in defined conditions.[18,21,27] Correia et al. showed that the vascular structures formed by human umbilical vein endothelial cells (HUVECs) were only stable when they were co-cultured with human MSCs (hMSCs).[20] In vivo studies have shown that endothelial cells co-cultured with hMSCs generate more robust vascular networks that can anastomose to the host vasculature.[28] Our group previously demonstrated that the co-culture of endothelial cells with hMSCs in a hydrogel significantly enhanced the formation of stable capillaries.[29,30]

Due to recent advances in microfabrication approaches, it is possible to integrate microvasculature in engineered tissues with spatial and temporal control over micropatterns.[31] Photocrosslinkable hydrogels provide flexibility to enhance architecture of the micropatterns.[32,33] Gelatin methacryloyl (GelMA) is a noncytotoxic and biodegradable hydrogel modified with methacryloyl groups, which has attracted significant attention in tissue engineering due to its photocrosslinkable properties and tunable mechanical robustness while retaining cell-binding motifs.[29,33–35] Interestingly, GelMA can be polymerized in vivo, allowing for the creation of vascular networks in situ.[36] GelMA constructs have been photopatterned to generate highly organized 3D vasculature through HUVECs encapsulation in the hydrogel prepolymer. It was shown that varying the width and height of beams could significantly alter HUVEC alignment within the micropatterned.[37] Although, an organized vasculature was formed by using this method, the potential of integrating the engineered vascular network with another tissue construct (e.g., bone) to engineer a vascularized tissue was not explored.

The objective of this work was to engineer a 3D construct with tunable angiogenic and osteogenic niches using photolithography and to study its potential for formation of vascularized bone tissue. This in vitro model enables investigating the effect of micropatterning of two different cell types in one construct and obtains further information on vascularization/bone tissue formation together in vitro.

2. Results and Discussion

2.1. Fabrication of Cell-Laden Micropatterned Constructs

Native bone tissue receives nutrients and oxygen through an organized vasculature. Therefore, engineering a functional bone tissue requires the formation of a biomimetic and organized vasculature.[2,15] We hypothesized that engineering a construct that permits simultaneous osteogenesis and angiogenesis in predefined patterns would address this challenge.[4,12] In this study, GelMA, which is a photopolymerizable hydrogel comprised of modified natural ECM components, was used as a material for both osteogenic and angiogenic niches. GelMA can be micropatterned using photolithography into a variety of shapes and configurations, without reducing cellular viability and function.[33,38–41]

A two-step photolithography process was used in this work to form spatially organized vascular networks inside an osteogenic niche (**Figure 1**).[42] Micropatterned vascular networks

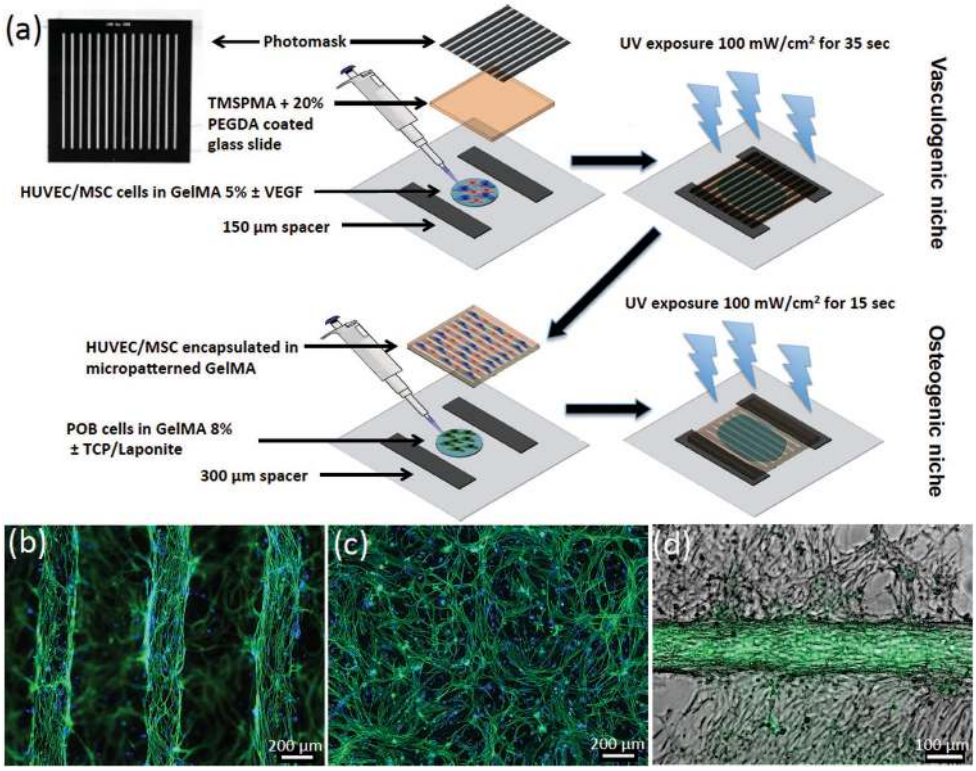

Figure 1. The application of photolithography technique to engineer photocrosslinkable three-component hydrogel constructs for creating 3D vascularized bone tissues. a) Schematic representation of cell-laden micropatterned vascular networks and osteogenic niche fabricated using direct polymerization through photomasks, b) micropatterned GelMA hydrogel containing HUVECs/hMSCs (1:1), c) actin filaments and DAPI stained HUVECs/hMSCs (1:1) encapsulated in unpatterned GelMA hydrogel, d) combined angiogenic niche containing HUVECs/hMSCs (1:1) co-culture in 5% GelMA and osteogenic niche containing POBs in 8% GelMA. The acronyms stand for: 3-(trimethoxysilyl)propyl methacrylate (TMSPMA), gelatin methacryloyl (GelMA), poly(ethylene glycol) diacrylate (PEGDA), mesenchymal stem cells (MSCs), human umbilical vein endothelial cells (HUVECs), tricalcium phosphate (TCP), and preosteoblasts (POBs).

were formed by encapsulating endothelial and MSCs inside GelMA in a precise and concentric fashion, strengthened by a secondary crosslinking step forming the osteogenic niche in GelMA (Figure 1). Although numerous approaches have been developed to create vascularized bone constructs,[29,43] relatively few studies have created biomimetic 3D bone architecture by forming endothelial cord-like vasculature within the bone forming hydrogel microstructure.

Several studies have shown that vascular endothelial growth factor (VEGF) recognized as an angiogenic protein regulates endothelial cell (i.e., HUVECs) proliferation and promote osteogenesis by reciprocal regulation between osteoblasts and endothelial cells.[5,18,44] It has been reported that hMSCs exhibit an angiogenic potential and considerable synergism when co-cultured with endothelial cells. However specifically defined media are essential to encourage hMSCs to differentiate into mural cells and colocalize with capillary-like structures. In terms of media ingredients, some studies have disputed VEGF as the most important growth factor regulating this differentiation.[18,45] Therefore the applied growth media in this work contained VEGF, endothelial cell growth medium (EGM-2 BulletKit, Lonza) in order to enhance vascularization while maintaining the growth of osteogenic cells. It has also been reported that co-delivering VEGF and osteogenic agents within separate niches enhances bone regeneration.[46] Therefore, the effect of loading both silicate nanoplatelets (Laponite) and tricalcium phosphate (βTCP) nanoparticles[47] into the osteogenic niche to induce osteogenesis was studied (Figure 1). We have previously reported that Laponite with large surface area (>350 m^2 g^{-1}) and ≈25 nm diameter and 1 nm thickness, possessing a negative face charge and a weak positive rim charge, are able to induce osteogenic differentiation in the absence of any additional osteoinductive factor.[48]

2.2. Development of the Angiogenic Niche

Encapsulated cells readily elongated, proliferated, and migrated when embedded in microfabricated GelMA hydrogels, indicating that the cells adhered to the hydrogel matrix. Cell alignment plays a critical role in many components of tissue microarchitecture. Several studies have reported cell alignment through local tension lines and along free boundaries such as grooved surfaces, microfibers, and micropatterns.[39,41,49–52] Here, we used a photomasking technique and micropatterned geometric restriction to create an aligned 3D spatial organization of vascular microstructures without the application of any additional stimuli.

Fluorescence images of HUVECs and hMSCs exhibited a rounded morphology of cells on day 1 and elongated and spindle-like morphology aligned along the direction of the micropatterns on day 3 (Figure 3a). On day 5 interconnection of neighboring cells with the formation of cord-like structure was observed on the patterned gels (Figure 1b). As expected, randomly distributed cells were observed within the unpatterned GelMA constructs (Figure 1c).

To investigate the effect of micropattern size on cellular alignment, HUVEC/hMSC-laden micropatterned hydrogels with varying beam widths (50, 150, and 300 m) were prepared using photolithography. The size of beam widths were selected based on the physiological size of small veins/large venules or small arteritis/large arterioles, which have lumen ranging about 50–300 m in diameter.[53–55]

Successful inclusion of homogeneously distributed cells within the micropatterns was confirmed by fluorescence microscopy. Within 5 d of culture, the microconstructs were filled with cells which aligned along the direction of the patterns which depended on the size of geometrical features, as shown by filamentous actin and nuclear staining (**Figure 2**a). It was observed that cellular alignment had an inverse relationship with dimension of the patterns. High degrees of cell alignment was observed for 50 m (up to 80% ± 7.6% for <10), and 150 m (up to 63% ± 2% for <10), while the 300 m beam size exhibited almost random orientation of cells and only those in close proximity to the perimeter tended to align along the long axis of the micropatterns (Figure 2b).

Confocal microscopy was used to assess 3D actin cytoskeleton organization and demonstrated that cells reorganized toward the periphery of the hydrogel constructs and self-assembled to form cord-like structures after 5 d of culture (Figure 2c). It should be noted that the structures as shown in Figure 2c are filled with hydrogel and are therefore not perfusable as is. We speculate that upon degradation of the hydrogel, open channels surrounded by endothelial cells should be attained. Optimal 3D cord and tubular structures with more circular cross-section profiles were observed for 150 m beam size (Video S1, Supporting Information). Therefore, constructs with 150 m geometrical feature was chosen for experiments. Studies have shown that when endothelial cells are patterned, mechanical stresses generated by traction forces will cause a higher stress concentrated on the periphery of the features. This in turn initiates patterned proliferation, which triggers tube morphogenesis during angiogenesis. This effect is critical after implantation as the luminal structure can connect to vasculature of the patient and contribute in nutrient transport and survival of the cells.[56]

To further assess the behavior of HUVECs and hMSCs when encapsulated individually or in co-culture in 150 m micropatterns, the cell filamentous actin and nuclei were stained after 1, 3, and 5 days of culture (**Figure 3**a). As shown in Figure 3b,c, both mono- and co-cultured cells were highly aligned and elongated in patterned GelMA hydrogel and no significant difference was observed between mono- and co-cultures. In patterned constructs on day 5, more than 85% and 95% of co-cultured cells were aligned at <10 and <20 deviation from the direction of the micropatterns axis, respectively. This result indicated that micropatterning can significantly enhance the cell alignment and elongation on both mono- and co-cultures within the hydrogel and form highly organized vascularized network. This is consistent with other in vitro and in vivo studies indicating the ability of MSCs to assist HUVECs in forming and maintaining a vascular network when co-cultured with hMSCs in a hydrogel. In a similar study by Tsigkou et al. much shorter

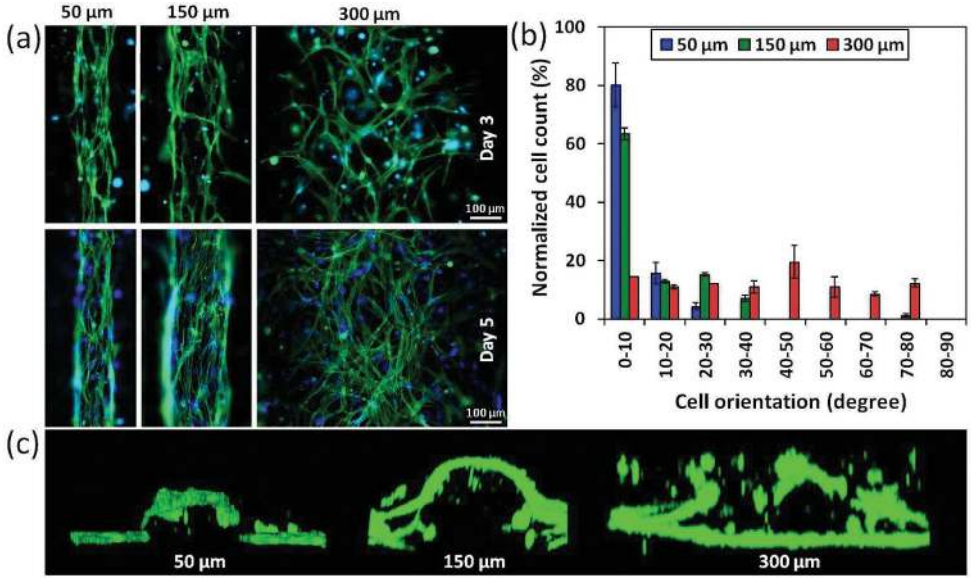

Figure 2. 3D cord formation and alignment of actin filaments (green) and DAPI (blue) stained HUVEC/hMSC in the micropattenred GelMA hydrogel. a) Effect of pattern size on cell alignment using HUVEC/hMSC-laden GelMA gel with 50 and 150 m micropatterned beams. b) Quantification of cell alignment at day 3 based on beam sizes. Error bars show the standard deviations between different trials. c) Representative confocal images (video can be viewed in the Supporting Information) from the cross-section of actin filaments stained HUVECs/hMCSs-laden micropatterned GelMA constructs, showing more stable 3D cord-like structure was created at 150 m (scale bars: 100 m).

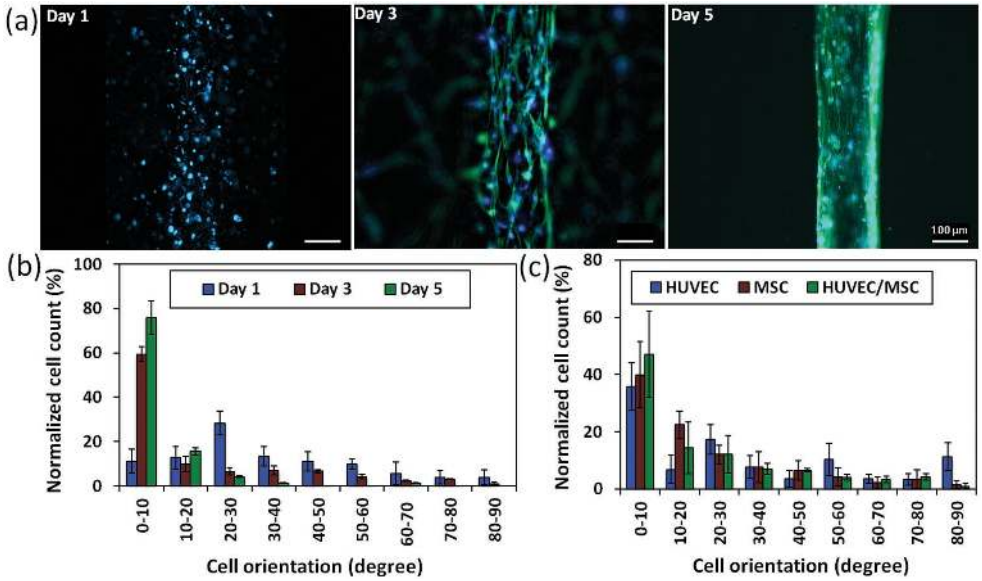

Figure 3. Cells cytoskeletal actin filaments alignment in 150 m micropatterned GelMA construct. Alignment analysis of cell within a) micropatterned regions of 5% (w/v) GelMA hydrogel after 1, 3, and 5 days of co-culture as obtained by photomasking technique. Representative fluorescence images demonstrate DAPI-stained cell nuclei with cytoskeletal actin filaments orientation within patterned regions of the hydrogel. b) Micropatterning significantly enhanced cell alignment in co-culture, more than 85% and 95% of co-cultured cells were aligned at <10 and <20 angles deviation from the direction of the micropatterns on day 5, respectively. c) Both mono- and co-cultured cells were aligned and elongated in patterned GelMA hydrogel (scale bars: 100 m).

and wider multicellular cords were reported in mono-cultures of HUVECs than those formed by hMSC-containing cultures.[5]

To investigate pattern fidelity, defined as the number of cells migrating from micropatterns, three groups of cell-laden samples were studied including mono-culture of green fluorescent protein (GFP)-HUVECs, hMSCs labeled with DiD (Vybrant, Thermo Fisher Scientific), and co-culture of GFP-HUVECs/hMSCs. Consequently the amount of migrated cells from micropatterns was calculated relative to the total number of cells. It was observed that hMSCs and GFP-HUVECs had the highest (≈55%) and lowest (≈10%) tendency to migrate respectively, with an intermediate value for cell migration for co-culture of GFP-HUVECs/MSCs (≈30%) (**Figure 4**). Overall, these data clearly indicate that the elongation, alignment, and migration responses could be controlled and directed through optimization of the micropatterning conditions and encapsulated cells.

Maintaining normal cellular behavior in a 3D microenvironment is an important criterion for the fabrication of tissue constructs.[49,57] The viability and proliferation of HUVECs and co-cultures of HUVECs/hMSCs with and without VEGF within micropatterns were assessed after 1, 3, and 5 days of culture. High viability of encapsulated cells was observed in patterned and unpatterned cell-laden GelMA and cells populated the constructs during the culture time. However, a significant increase in cellular metabolic activity and proliferation in co-cultures was observed as compared to HUVECs mono-cultures on day 5 as shown by a PrestoBlue assay (**Figure 5**b). This proliferation pattern was confirmed by measuring the total cell quantification of 4′,6-diamidino-2-phenylindole (DAPI)-stained cells (Figure 5c). Over 90% cell viability was observed within the microconstructs by using a LIVE/DEAD assay as shown in Figure 5a, confirming the cytocompatibility of the fabrication process.

It is known that crosstalk between endothelial cells and hMSCs can direct the differentiation of stem cells toward smooth muscle cells that later wrap endothelialized channels to form functional vessels. Thus, we performed immunostaining against an endothelial marker (CD31) and a smooth muscle marker (αSMA). CD31, known as platelet endothelial cell adhesion molecule 1, is expressed on the surface of endothelial cell intercellular junctions. αSMA is a marker for mural cells and is a major constituent of the contractile apparatus within these cells. Contractile cytoskeletal protein αSMA is the earliest marker of smooth muscle cell differentiation, which is present in both small and large blood vessels. The micropatterned constructs were CD31 and αSMA positive at day 5 by immunostaining (Figure 5d,e,f). The expression of αSMA confirmed that hMSCs differentiated to mural cells to stabilize the engineered vascular network. We have previously shown that co-culturing of hMSCs and HUVECs in hydrogel resulted in the formation of these stabilized vascular networks but the vasculature was randomly generated in bulk GelMA hydrogel.[58] To further assess the vascular stability, the expression of endothelial intercellular junctional protein VE-cadherin was examined after two weeks of culture (**Figure 6**b). Visualization of CD31 and VE-cadherin within the micropatterned hydrogel constructs confirmed that the HUVECs co-cultured with hMSCs formed vascular structures that exhibited mature intercellular junctions. Thus, micropatterning enabled us to engineer more organized vascular networks with the micropatterned HUVEC/hMSC-laden GelMA gel.

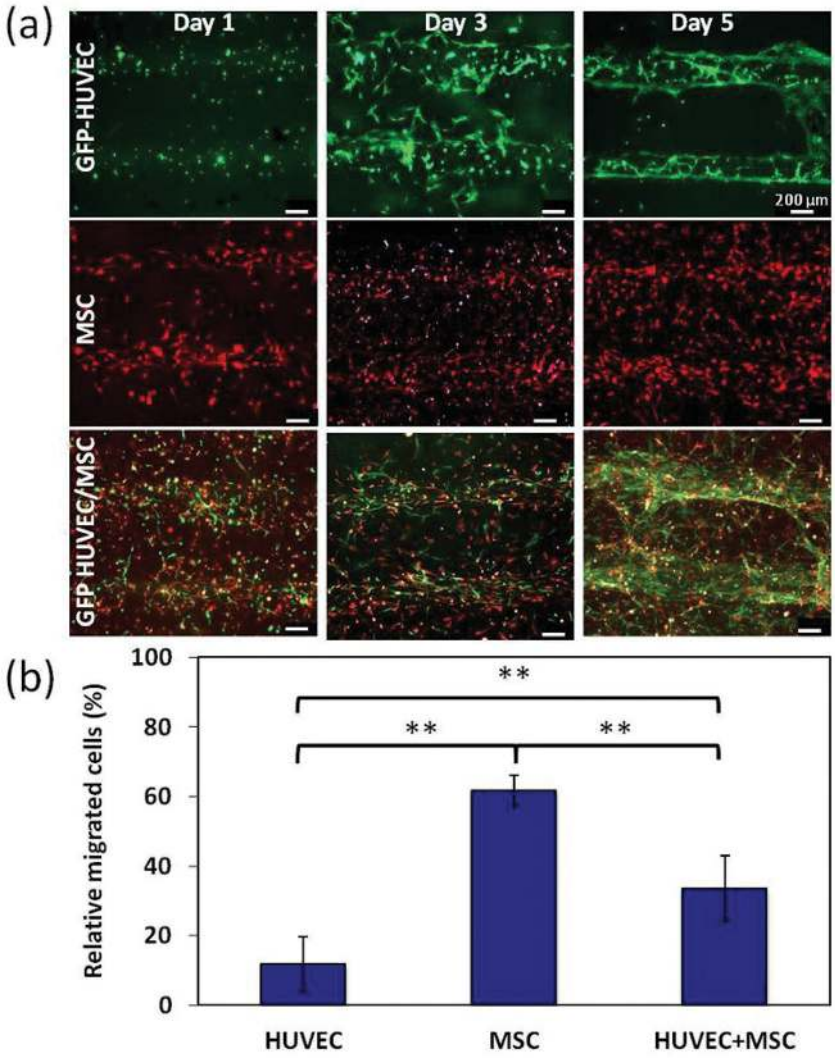

Figure 4. Cell migration from micropatterns. a) Cell migration after 1, 3, and 5 d. b) Quantification of relative migrated cells after 3 d. Relative migration indicates the relative number of migrated cells to the total number of cells. hMSCs and GFP-HUVECs showed the highest (≈55%) and lowest (≈10%) tendency to migrate and GFP-HUVECs/MSCs coculture was somewhat in between (≈30%). Columns indicate the values from six experiments; bars, SD. $^{**}P < 0.01$ as compared (scale bars: 200 m).

2.3. Formation of the Vascularized Bone Tissue Constructs

Higher concentration of GelMA (8%(w/v)) was utilized to form osteogenic constructs including preosteoblasts (POB)-laden hydrogel around micropatterned vascular network. This results in a higher stiffness for the osteogenic environment, which has been shown to be beneficial for the osteogenic differentiation of hMSC.[59] The fabrication of combined angiogenic and osteogenic niches was successfully achieved with a two-step process, where HUVECs/hMSCs-laden micropattered GelMA lines were covered with a layer of POB-encapsulated GelMA hydrogel (Figure 6a). The construct was then cultured in the EGM2 media for 21 d.

The osteogenic differentiation in the POB-laden GelMA regions was confirmed by staining the calcified matrix with Alizarin Red (Figure 6c,d). This mineralization assay demonstrated high Alizarin Red absorbance from samples containing βTCP in comparison to Laponite and control. However this difference was expected due to the high concentration of calcium in βTCP as confirmed by a control with βTCP but without cells. Although mineralization was not significant in comparison to the control but stronger POB osteoinduction was observed from silicate nanoparticles (Laponite) in comparison to βTCP nanoparticles. Real-time polymerase chain reaction (qPCR) analysis indicated that osteogenic genes, such as osteocalcin (OCN), RUNX2, osteopontin (OPN), and alkaline phosphatase (ALP), were upregulated in the engineered osteogenic-matrix after inclusion of βTCP or Laponite at day 21. Significant upregulation of OCN and OPN was observed in the osteogenic niche after combination of the angiogenic niche and osteogenic niche (Combo) (Figure 6e). This is consistent with previous literature showing that co-cultures of hMSC and endothelial cells result in an increased osteogenic differentiation due to growth factor interactions.[10,20,21] The results indicated that while the HUVECs/hMSCs-laden micropattered GelMA held a great potential to generate highly organized and mature vascular networks with a level of maturity indicated by the presence of VE-Cadherin between neighboring endothelial cells (Figure 6b), the POB-encapsulated GelMA could maintain their regular differentiation functions (Figure 6e) and generate osteogenesis simultaneously in culture medium, which does not contain osteogenic factors.

3. Conclusions

This study presents a method to pattern vascular structures within a tissue engineered bone construct using a two-step photopolymerization approach. This approach offers a high level of control over the organization of the vascular structures, especially when patterns with a width of 150 m or less are used. By adapting the design of the photomasks used, this potentially enables the design of complex vascular patterns resembling for instance a vascular tree. hMSCs present in the angiogenic niche differentiate toward mural cells and stabilize the vascular structures. By adding Laponite silicate nanoparticles to the osteogenic niche, MC3T3s in the osteogenic niche maintain their osteogenic potential, even when cultured in media not supplemented with osteogenic factors. The osteogenic differentiation is further increased by the presence of angiogenic niche containing endothelial cells.

This study shows the potential of engineering a tissue containing two separate niches, which are optimized for their respective function. By localizing tissue developmental cues, our

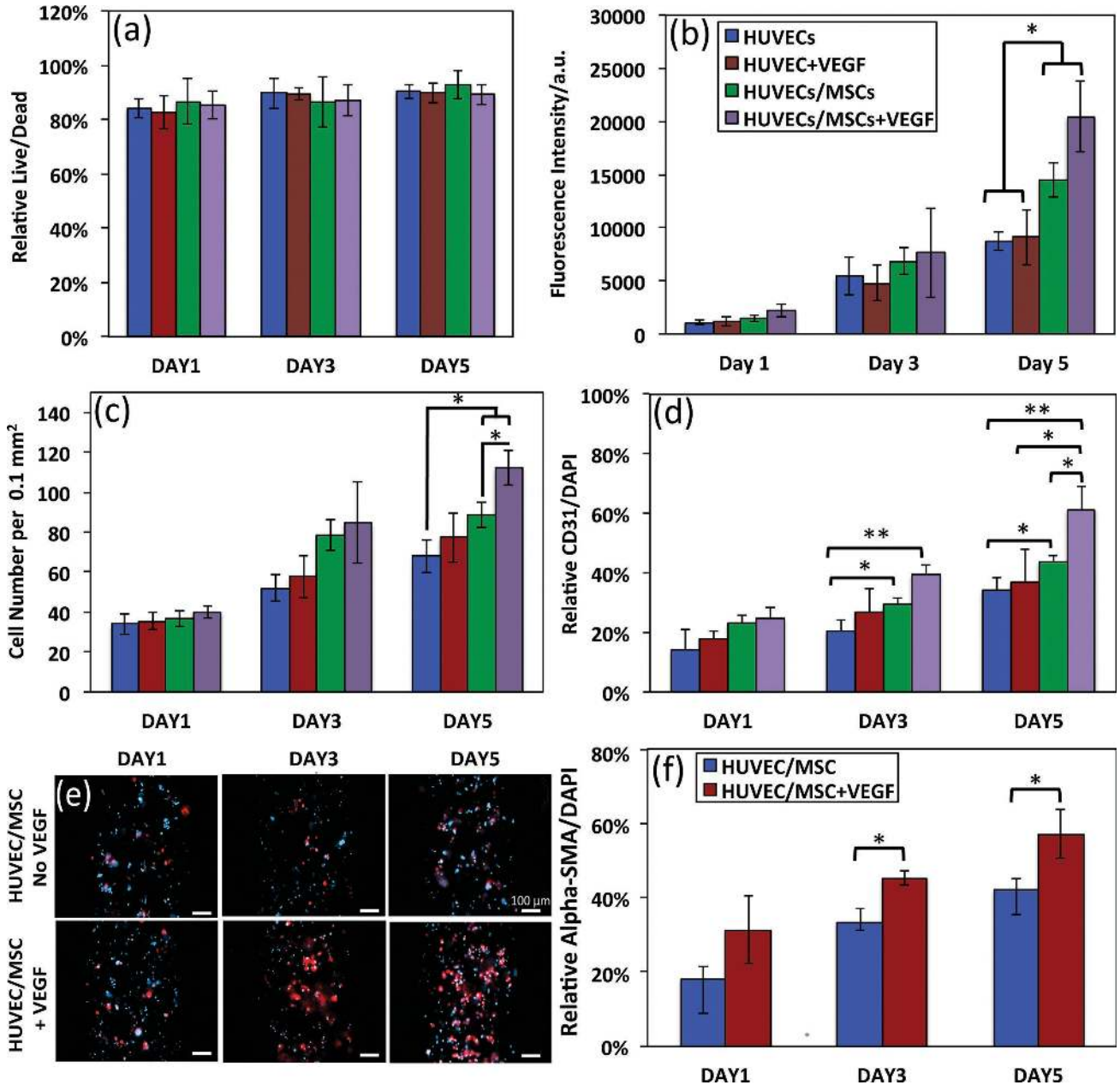

Figure 5. Cellular behavior in a 3D microenvironment. a) Live/dead cell viability assay shows >90% viability after 5 d. b) PrestoBlue metabolic assay indicates significant proliferation of coculture. c) Total cell quantification of DAPI-stained cells confirms the high proliferation. d) Higher amount of CD31 expression was observed in the coculture indicating higher endothelial activity. e) Effect of VEGF on α-SMA expression (red) in HUVEC/hMSC coculture; blue is showing cell nuclei. f) Quantification of relative α-SMA shows higher expression of α-SMA, defined as the percentage of cell nuclei that colocalize with positive staining for α-SMA. Columns indicate the values from six experiments; bars, SD. $*p < 0.05$ and $**p < 0.01$ as compared.

approach enables the formation of multiple tissue structures within a single construct cultured in a single medium. This is an important advancement for multistructural tissue engineering where the inclusion of a vascular or neural network is essential.

4. Experimental Section

Synthesis of GelMA and Prepolymer: GelMA was synthesized according to our previous work.[33,50] Medium methacrylation degree of GelMA (53.8% ± 0.5%) was selected due to its robust mechanical properties and low mass swelling ratio at low UV exposure which provided high cell viability.[33,60] Briefly, GelMA was produced by dissolving 10% (w/v) type A gelatin derived from porcine skin (Sigma-Aldrich) into Dulbecco's phosphate buffered saline (DPBS) (GIBCO) by stirring at 50 C. Then 5 mL methacrylic anhydride (MA) (Sigma-Aldrich) was added dropwise to the suspension at a rate of 0.5 mL min^{-1} and allowed to stir for 3 h at 50 C. The addition of methacrylate groups to the amine-side groups of gelatin created a photopolymerizable hydrogel.[33,39] Subsequently, the reaction was stopped by diluting the solution fivefold with Dulbecco's phosphate-buffered saline (DPBS) at 50 C. The GelMA

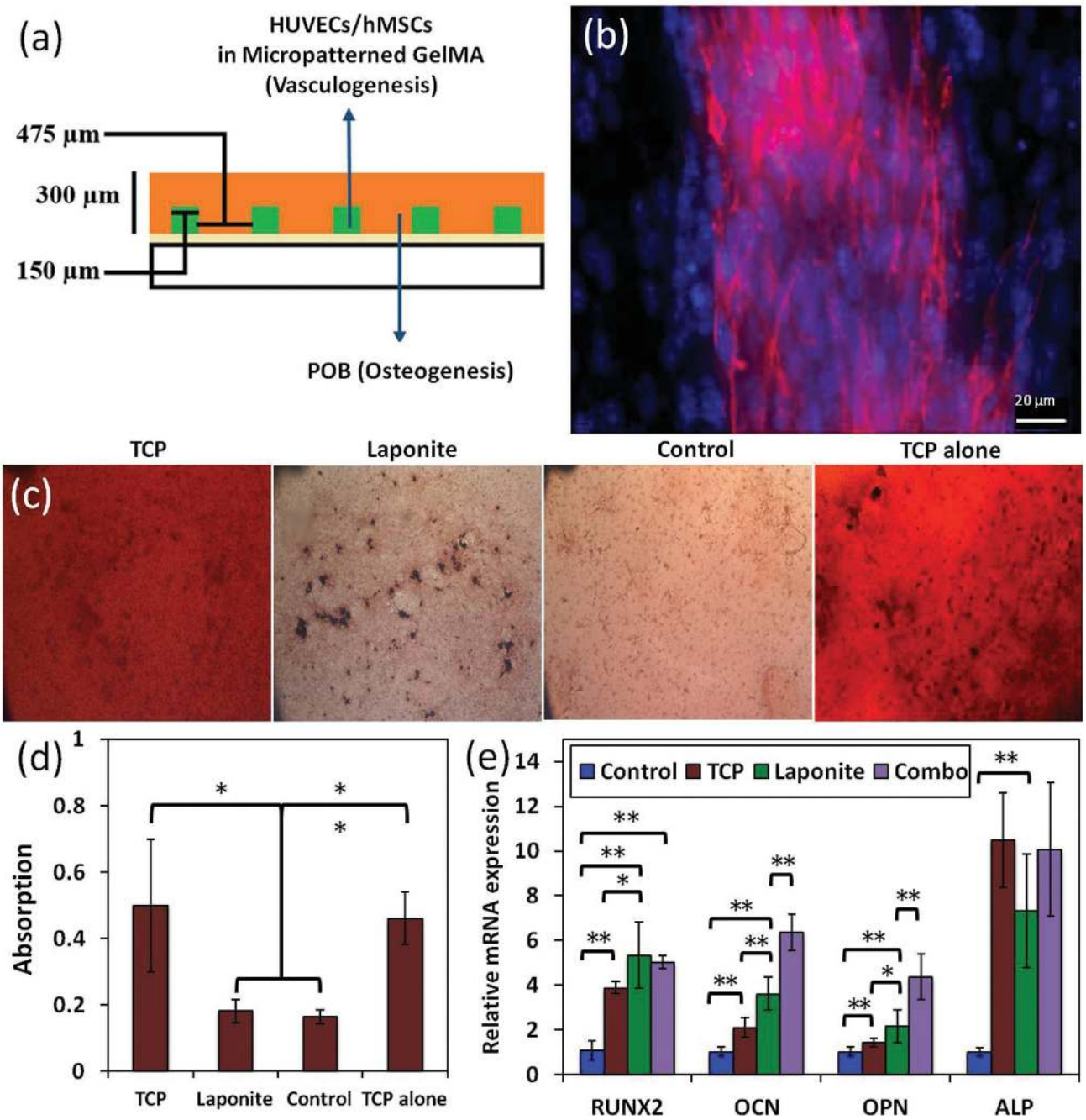

Figure 6. Characterization of the engineered vasculo-osteogenic constructs. a) Schematic of vasculo-osteogenic construct. b) Expression of endothelial intercellular junctional protein VE-cadherin after 2 weeks culture. c) Representative Alizarin Red images of POB-laden osteogenic GelMA constructs with βTCP or Laponite. d) Significantly higher calcium deposition was observed in the samples with βTCP ($^*P < 0.05$), this difference was due to the presence of calcium in βTCP as confirmed by βTCP sample without cells. e) qPCR analysis indicated that osteogenic genes OCN, RUNX2, OPN, and ALP were expressed in the engineered osteogenic-matrix and significant upregulation of OCN and OPN was observed in the osteogenic niche after combination of angiogenic niche and osteogenic niche (Combo) at day 21. The acronyms stand for: tricalcium phosphate (βTCP), preosteoblasts (POBs), mesenchymal stem cells (MSCs), human umbilical vein endothelial cells (HUVECs), runt-related transcription factor 2 (RUNX2), osteocalcin (OCN), osteopontin (OPN), and alkaline phosphatase (ALP).

solution was then dialyzed against distilled water for 10 d using a 12–14 kDa cutoff dialysis tube (Spectrum Laboratories) to remove salts and unreacted MA. After freezing the GelMA solution at –80 C, a white GelMA foam was obtained by lyophilization and stored at –20 C. GelMA prepolymer solution was prepared by mixing freeze-dried GelMA foam at concentrations of 5% and 8% (w/v) and the photoinitiator [2-hydroxy-1-(4-(hydroxyethoxy) phenyl)-2-methyl-1-propanone, Irgacure 2959] (CIBA Chemicals) in DPBS at 80 C.

Micropatterning Process: A two-step microfabrication protocol was developed with angiogenic and osteogenic niches in a single construct. First, to make GelMA prepolymer adhere to the glass slides (1 cm^2), free methacrylate groups were created on the slides by treating the

glass with 3-(trimethoxysilyl)propyl methacrylate (TMSPMA) (Sigma) according to a previously described protocol.[33] TMSPMA-treated slides were sterilized by UV light prior to experiments. To generate the micropatterned angiogenic niche, 20 L GelMA 5% (w/v) solution containing GFP-HUVECs and hMSCs at a cell densities of 2.5×10^6 and 2.5×10^6 cells mL^{-1}, respectively, was added between the 150 m spacers on a petri dish and covered with a TMSPMA-treated glass slide. To create an organized array of GelMA micropatterns on the glass, a photomask with 475 m spacing and 50, 150, and 300 m beam size (designed by AutoCAD software) was positioned on top of the slide and the cell-encapsulated GelMA was photocrosslinked with UV light positioned beneath the device (OmniCure Series 2000) with 100 mW cm^{-2} for 35 s. A photomask is a 2D pattern printed onto a transparent sheet, designed such that light only passes through the mask in specific patterns (Figure 1).[42] The osteogenic niche was overlaid on the micropatterned GelMA on TMSPMA glass as a layer of POB laden GelMA 8% (w/v) at a cell density of 5×10^6 cells mL^{-1} with 300 m spacers and polymerized with UV light with 100 mW cm^{-2} for 35 s. The GelMA/POB layer filled the spaces between the micropatterned angiogenic lines intended for bone formation and generated a construct for osteogenesis through differentiation of POB to mature osteoblasts in the presence of optimized endothelial cell growth media (Figure 1). The construct was then cultured in the EGM-2 media.

Cell Culture: GFP-expressing HUVECs (Lonza) were cultured in basal medium (EBM-2; Lonza) and supplemented with endothelial growth BulletKit (EGM-2; Lonza). Human bone marrow-derived mesenchymal stem cells (hMSCs) (Lonza) were cultured in minimum essential medium alpha (MEM Alpha, Life Technologies) and supplemented with 2×10^{-3} M L-glutamine (Life Technologies), 0.2 M ascorbic acid (Life Technologies), 1 ng mL^{-1} basic fibroblast growth factor (bFGF, Life Technologies), 10% fetal bovine serum (FBS, Life Technologies), and 1% antibiotic-antimycotic (Gibco). MC3T3 preosteoblast cells (POBs) were cultured using the growth media, containing minimum essential medium alpha supplemented with 10% fetal bovine serum and 1% antibiotic-antimycotic. The cells with passage numbers between 3 and 6 were used in the experiments. The media were changed every 2 d and the cells were passaged at 80% confluency. For cell encapsulation, the cells were trypsinized, counted, and homogenously mixed with 37 C GelMA solution and used immediately.

Quantification of Cellular Alignment: The cell-laden hydrogels were fixed in 4% paraformaldehyde solutions in DPBS and stained with phalloidin (Alexa-Fluor 488, Invitrogen) and DAPI (Invitrogen) according to the manufacturer's instructions. Briefly, the specimen were permeabilized with 0.3% (v/v) Triton X-100 for 15 min and blocked by using 5% (w/v) bovine serum albumin (BSA) for 60 min before staining. Alignment analysis was performed using fluorescent images with an inverted fluorescence microscope (Nikon TE 2000-U, Nikon instruments, USA) to reveal filamentous actin and cell nuclei. The cellular alignment within patterned regions of the hydrogels was quantified based on cytoskeletal actin filaments-stained fluorescent images according to a previously described procedure.[40,51,61] To quantify the overall cellular alignment for each sample, the alignment of actin filaments in the encapsulated was grouped in 10 increments and the alignment distributions were normalized to the respective preferred orientation to defined mean orientation. The measurements were performed using the built-in functions of ImageJ software (National Institutes of Health (NIH)) (six images for each sample) (Figure 2). Confocal microscopy was used to evaluate actin cytoskeletal organization of the micropatterns (Video S1, Supporting Information).

Cell Viability and Proliferation Assay: In vitro qualitative analysis of viability of the encapsulated cells in GelMA constructs was performed using the fluorescence-based LIVE/DEAD viability/cytotoxicity assay kit (Invitrogen) consisting intracellular green-fluorescent calcein AM and red-fluorescent ethidium homodimer. Initially a solution containing two components at 0.5 L mL^{-1} of calcein and 2 L mL^{-1} ethidium homodimer was dissolved in DPBS, respectively. At each time point the media were removed and the hydrogels covered with cells were rinsed with DPBS and subsequently 1 mL of the solution was added to each sample. After incubation for 30 min at ambient condition, the samples were imaged with 10× magnifications using an inverted fluorescent microscope (Nikon TE 2000-U, Nikon instruments, USA). Total number of cells (red and green) and number of live cells (green) were counted using ImageJ software (NIH). Finally, cell viability was quantified by dividing the number of live cells by total number of cells. The calculations were based on three independent samples and reported based on the mean ± standard deviation (SD) (Figure 3). Cell proliferation was assessed using resazurin-based PrestoBlue assay (Invitrogen), a nontoxic metabolic indicator for viable cells. Briefly, after each time point the culture medium was removed and the samples were rinsed with DPBS. Subsequently the medium containing 10% PrestoBlue reagent was added to each well and incubated at 37 C for 1 h. The samples with reagent but no cells served as the blank control. The fluorescence of the reduced PrestoBlue dye was read at 570 (excitation) and 600 nm (emission) with a microplate reader (Biotek, USA), and all values were corrected based on blank control. Three replicates were analyzed for 1, 3, and 5 days and growth was plotted based on the mean ± standard deviation (six images for each sample).

Immunostaining: The angiogenic activity of HUVECs/hMSCs coculture was investigated using fluorescent microscopy to assess CD31 and α-SMA expression. The samples were rinsed in DPBS and fixed in 4% paraformaldehyde solution in DPBS for 20 min. Subsequently the cell membranes were permeabilized in 0.1% Triton X-100 in DPBS for 15 min and washed with DPBS for three times. The samples were then blocked with 1% (w/v) BSA in DPBS for 1 h, followed by primary antibody staining with 1/40 dilution of rabbit monoclonal anti-CD31 antibody (Abcam) and 1/100 dilution of mouse monoclonal antialpha smooth muscle actin antibody (Abcam) in 0.1% BSA blocking solution overnight at 4 C. The samples were washed in DPBS three times with 1 h intervals in between the washing steps. After primary antibody staining, the samples were incubated in 1/200 dilution of Alexa Fluor-488 conjugated goat antirabbit (Abcam) and 1/200 dilution of Alexa Fluor-594 conjugated goat antimouse secondary antibodies (Abcam) in 0.1% BSA in DPBS for 2 h at ambient condition. Subsequently, the samples were washed in DPBS three times with 1 h intervals in between the washing steps, followed by 1/1000 dilution DAPI staining for 5 min. After rinsing the samples with DPBS, fluorescent images were taken. The relative surface area of coverage for stains was quantified with the ImageJ software (NIH). The images for the expression of VE-cadherein (Abcam) as the primary antibody within the micropatterned regions of GelMA hydrogel constructs were assessed after 21 days culture using the same protocol as described above.

Mineralization: The cell-laden constructs were fixed using 4% paraformaldehyde for 30 min at room temperature after washing twice with PBS. Subsequently, the samples were stained for 10 min with 2% Alizarin Red (Sigma-Aldrich) solution of which the pH was adjusted to 4.1–4.3 using ammonium hydroxide. The samples were then washed with distilled water several times to remove all untreated reagents. Stained slides were visualized by phase microscopy using an inverted microscope (Nikon). To quantify mineralization, the sample were dissolved in 200 L ammonia solution (10%) and kept overnight. Following vortexing, the solution was heated at 80 C for 10 min and centrifuged at 20 000 × *g* for 15 min. Afterward 75 L of 10% ammonia solution was added to each solution and the absorbance was read at 405 nm.

RNA Isolation and Quantitative Real-Time PCR (qPCR): Total RNA was extracted from samples using TRIzol (Invitrogen) and 1 g of total RNA was used for cDNA synthesis with SuperScriptTM III First-Strand Synthesis SuperMix (Invitrogen). For quantitative real-time PCR analysis, gene-specific primers were designed to amplify mouse RUNX2, OPN, OCN, ALP, and the housekeeping gene glyceraldehyde 3-phosphate dehydrogenase (GAPDH). Primer pairs are as follows: RUNX2 (5′-AGG TTG GAG GCA CAC ATA GG-3′, 5′-TTG ACC TTT GTC CCA ATG C-3′), OPN (5′-AAG CAT CCT TGC TTG GGT TT-3′, 5′-CAG GCT TAC CTT GGC TGG TTT-3′), OCN (5′-ATT TAG GAC CTG TGC TGC CC-3′, 5′-GCA GAG AGA GAG GAC AGG GA-3′), ALP (5′-CAG GCC GCC TTC ATA AGC A-3′, 5′-AAT TGA CGT TCC GAT CCT GC-3′), and GAPDH (5′-ACA CAT

TGG GGG TAG GAA CA-3′, 5′-AAC TTT GGC ATT GTG GAA GG-3′). All amplifications were performed in a final reaction mixture (20 L) containing 1 final concentration of Bio-Rad SYBR Green Master Mix (Bio-Rad, Hercules, CA), 500 nmol L^{-1} of gene-specific primers, and 1 L of template, using the following conditions: an initial denaturation at 95 C for 1 min, followed by 45 cycles of 95 C for 15 s, 56 C for 15 s, and 72 C for 15 s, with a final extension at 72 C for 5 min. After amplification, the baseline and threshold levels for each reaction were determined using CFX Manager™ Software (Bio-Rad). For validation of polymerase chain reaction (PCR), amplified products were separated on 1% agarose gels and visualized by ethidium bromide staining. The relative quantification in gene expression was determined using the $2^{-\Delta\Delta}$Ct method.[62]

Statistical Analysis: The statistical significance was determined by an independent Student *t*-test for two groups of data or analysis of variance. Data were calculated as mean ± standard deviation for six replicates and *p*-values were presented as statistically significant and highly significant as $*p < 0.05$, $**p < 0.01$, respectively.

Supporting Information

Supporting Information is available from the Wiley Online Library or from the author.

Acknowledgements

The authors acknowledge funding from the National Science Foundation (EFRI-1240443), IMMODGEL (602694), and the National Institutes of Health (EB012597, AR057837, DE021468, HL099073, AI105024, and AR063745). J.R. was supported by the People Programme (Marie Curie Actions) of the European Union's Seventh Framework Programme (FP7/2007–2013) under Research Executive Agency (REA) Grant Agreement No. 622294.

Received: October 2, 2016
Revised: December 20, 2016
Published online: February 27, 2017

[1] Á. Mercado-Pagán, A. Stahl, Y. Shanjani, Y. Yang, *Annu. Biomed. Eng.* **2015**, *43*, 718.
[2] M. I. Santos, R. L. Reis, *Macromol. Biosci.* **2010**, *10*, 12.
[3] C. F. Lord, M. C. Gebhardt, W. W. Tomford, H. J. Mankin, *J. Bone Jt. Surg.* **1988**, *70*, 369.
[4] K. J. L. Burg, S. Porter, J. F. Kellam, *Biomaterials* **2000**, *21*, 2347.
[5] O. Tsigkou, I. Pomerantseva, J. A. Spencer, P. A. Redondo, A. R. Hart, E. O'Doherty, Y. Lin, C. C. Friedrich, L. Daheron, C. P. Lin, C. A. Sundback, J. P. Vacanti, C. Neville, *Proc. Natl. Acad. Sci. USA* **2010**, *107*, 3311.
[6] S. Bose, M. Roy, A. Bandyopadhyay, *Trends Biotechnol.* **2012**, *30*, 546.
[7] M. K. Narbat, M. S. Hashtjin, M. Pazouki, *Iran. J. Biotechnol.* **2006**, *4*, 54.
[8] N. A. Beckmann, S. Mueller, M. Gondan, S. Jaeger, T. Reiner, R. G. Bitsch, *J. Arthroplasty* **2015**, *30*, 249.
[9] H. Nie, M.-L. Ho, C.-K. Wang, C.-H. Wang, Y.-C. Fu, *Biomaterials* **2009**, *30*, 892.
[10] J. Ma, S. K. Both, F. Yang, F. Z. Cui, J. Pan, G. J. Meijer, J. A. Jansen, J. J. van den Beucken, *Stem Cells Transl. Med.* **2014**, *3*, 98.
[11] S. P. Bruder, B. S. Fox, *Clin. Orthop. Relat. Res.* **1999**, *367*, S68.
[12] L. H. Nguyen, N. Annabi, M. Nikkhah, H. Bae, L. Binan, S. Park, Y. Kang, Y. Yang, A. Khademhosseini, *Tissue Eng., Part B* **2012**, *18*, 363.
[13] Y. Liu, B. Moller, J. Wiltfang, P. H. Warnke, H. Terheyden, *Tissue Eng., Part A* **2014**, *20*, 3189.
[14] R. K. Jain, P. Au, J. Tam, D. G. Duda, D. Fukumura, *Nat. Biotechnol.* **2005**, *23*, 821.
[15] L. Krishnan, N. Willett, R. Guldberg, *Ann. Biomed. Eng.* **2014**, *42*, 432.
[16] a) E. C. Novosel, C. Kleinhans, P. J. Kluger, *Adv. Drug Delivery Rev.* **2011**, *63*, 300; b) M. O. Wang, C. E. Vorwald, M. L. Dreher, E. J. Mott, M.-H. Cheng, A. Cinar, H. Mehdizadeh, S. Somo, D. Dean, E. M. Brey, J. P. Fisher, *Adv. Mater.* **2015**, *27*, 138.
[17] H. R. Nejad, Z. G. Malekabadi, M. K. Narbat, N. Annabi, P. Mostafalu, F. Tarlan, Y. S. Zhang, M. Hoorfar, A. Tamayol, A. Khademhosseini, *Small* **2016**, *12*, 5132.
[18] J. García, A. García, *Drug Delivery Transl. Res.* **2015**, *1*, 77.
[19] N. Annabi, A. Tamayol, J. A. Uquillas, M. Akbari, L. E. Bertassoni, C. Cha, G. Camci-Unal, M. R. Dokmeci, N. A. Peppas, A. Khademhosseini, *Adv. Mater.* **2014**, *26*, 85.
[20] C. Correia, W. L. Grayson, M. Park, D. Hutton, B. Zhou, X. E. Guo, L. Niklason, R. A. Sousa, R. L. Reis, G. Vunjak-Novakovic, *PloS One* **2011**, *6*, e28352.
[21] J. M. Kanczler, R. O. Oreffo, *Eur. Cells Mater.* **2008**, *15*, 100.
[22] S. Patan, in *Angiogenesis in Brain Tumors*, Vol. *117* (Eds: M. Kirsch, P. Black), Springer, Norwell, USA, **2004**, p. 3.
[23] U. Blache, S. Metzger, Q. Vallmajo-Martin, I. Martin, V. Djonov, M. Ehrbar, *Adv. Healthcare Mater.* **2016**, *5*, 489.
[24] D. Barati, S. R. Shariati, S. Moeinzadeh, J. M. Melero-Martin, A. Khademhosseini, E. Jabbari, *J. Controlled Release* **2016**, *223*, 126.
[25] B. V. Slaughter, S. S. Khurshid, O. Z. Fisher, A. Khademhosseini, N. A. Peppas, *Adv. Mater.* **2009**, *21*, 3307.
[26] C. S. Choong, D. W. Hutmacher, J. T. Triffitt, *Tissue Eng.* **2006**, *12*, 2521.
[27] R. Vattikuti, D. A. Towler, *Am. J. Phys.: Endocrinol. Metab.* **2004**, *286*, E686.
[28] D. M. Supp, K. Wilson-Landy, S. T. Boyce, *FASEB J.* **2002**, *16*, 797.
[29] Y.-C. Chen, R.-Z. Lin, H. Qi, Y. Yang, H. Bae, J. M. Melero-Martin, A. Khademhosseini, *Adv. Funct. Mater.* **2012**, *22*, 2027.
[30] W.-H. Yeo, Y.-S. Kim, J. Lee, A. Ameen, L. Shi, M. Li, S. Wang, R. Ma, S. H. Jin, Z. Kang, Y. Huang, J. A. Rogers, *Adv. Mater.* **2013**, *25*, 2773.
[31] H. Kaji, presented at *Int. Symp. Micro-NanoMechatronics Hum. Sci. (MHS)*, Nagoya, Japan, November **2012**.
[32] Y. Zuo, W. Xiao, X. Chen, Y. Tang, H. Luo, H. Fan, *Chem. Commun.* **2012**, *48*, 3170.
[33] J. W. Nichol, S. T. Koshy, H. Bae, C. M. Hwang, S. Yamanlar, A. Khademhosseini, *Biomaterials* **2010**, *31*, 5536.
[34] P. Hassanzadeh, M. Kazemzadeh-Narbat, R. Rosenzweig, X. Zhang, A. Khademhosseini, N. Annabi, M. Rolandi, *J. Mater. Chem. B* **2016**, *4*, 2539.
[35] M. Kazemzadeh-Narbat, N. Annabi, A. Khademhosseini, *Mater. Today* **2015**, *18*, 176.
[36] R. Z. Lin, Y. C. Chen, R. Moreno-Luna, A. Khademhosseini, J. M. Melero-Martin, *Biomaterials* **2013**, *34*, 6785.
[37] M. Nikkhah, F. Edalat, S. Manoucheri, A. Khademhosseini, *Biomaterials* **2012**, *33*, 5230.
[38] a) H. Qi, Y. Du, L. Wang, H. Kaji, H. Bae, A. Khademhosseini, *Adv. Mater.* **2010**, *22*, 5276; b) N. Annabi, K. Tsang, S. M. Mithieux, M. Nikkhah, A. Ameri, A. Khademhosseini, A. S. Weiss, *Adv. Funct. Mater.* **2013**, *23*, 4950; c) W. Xiao, J. He, J. W. Nichol, L. Wang, C. B. Hutson, B. Wang, Y. Du, H. Fan, A. Khademhosseini, *Acta Biomater.* **2011**, *7*, 2384.
[39] J. Ramon-Azcon, S. Ahadian, R. Obregon, G. Camci-Unal, S. Ostrovidov, V. Hosseini, H. Kaji, K. Ino, H. Shiku, A. Khademhosseini, T. Matsue, *Lab Chip* **2012**, *12*, 2959.

[40] J. Ramon-Azcon, S. Ahadian, R. Obregon, G. Camci-Unal, S. Ostrovidov, V. Hosseini, H. Kaji, K. Ino, H. Shiku, A. Khademhosseini, T. Matsue, *Lab Chip* **2012**, *12*, 2959.
[41] a) R. Gauvin, Y. C. Chen, J. W. Lee, P. Soman, P. Zorlutuna, J. W. Nichol, H. Bae, S. Chen, A. Khademhosseini, *Biomaterials* **2012**, *33*, 3824; b) H. Aubin, J. W. Nichol, C. B. Hutson, H. Bae, A. L. Sieminski, D. M. Cropek, P. Akhyari, A. Khademhosseini, *Biomaterials* **2010**, *31*, 6941.
[42] T. I. Son, M. Sakuragi, S. Takahashi, S. Obuse, J. Kang, M. Fujishiro, H. Matsushita, J. Gong, S. Shimizu, Y. Tajima, Y. Yoshida, K. Suzuki, T. Yamamoto, M. Nakamura, Y. Ito, *Acta Biomater.* **2010**, *6*, 4005.
[43] a) N. Koike, D. Fukumura, O. Gralla, P. Au, J. S. Schechner, R. K. Jain, *Nature* **2004**, *428*, 138; b) J. M. Melero-Martin, M. E. De Obaldia, S. Y. Kang, Z. A. Khan, L. Yuan, P. Oettgen, J. Bischoff, *Circ. Res.* **2008**, *103*, 194.
[44] Y.-Q. Yang, Y.-Y. Tan, R. Wong, A. Wenden, L.-K. Zhang, A. B. M. Rabie, *Int. J. Oral. Sci.* **2012**, *4*, 64.
[45] H. Bae, A. S. Puranik, R. Gauvin, F. Edalat, B. Carrillo-Conde, N. A. Peppas, A. Khademhosseini, *Sci. Transl. Med.* **2012**, *4*, 160ps23.
[46] M. M. Deckers, M. Karperien, C. van der Bent, T. Yamashita, S. E. Papapoulos, C. W. Lowik, *Endocrinology* **2000**, *141*, 1667.
[47] a) H. Yuan, Z. Yang, Y. Li, X. Zhang, J. D. De Bruijn, K. De Groot, *J. Mater. Sci.: Mater. Med.* **1998**, *9*, 723; b) C. Weinand, I. Pomerantseva, C. M. Neville, R. Gupta, E. Weinberg, I. Madisch, F. Shapiro, H. Abukawa, M. J. Troulis, J. P. Vacanti, *Bone* **2006**, *38*, 555.
[48] a) A. K. Gaharwar, S. M. Mihaila, A. Swami, A. Patel, S. Sant, R. L. Reis, A. P. Marques, M. E. Gomes, A. Khademhosseini, *Adv. Mater.* **2013**, *25*, 3329; b) J. I. Dawson, J. M. Kanczler, X. B. Yang, G. S. Attard, R. O. Oreffo, *Adv. Mater.* **2011**, *23*, 3304.
[49] S. R. Shin, B. Aghaei-Ghareh-Bolagh, T. T. Dang, S. N. Topkaya, X. Gao, S. Y. Yang, S. M. Jung, J. H. Oh, M. R. Dokmeci, X. S. Tang, A. Khademhosseini, *Adv. Mater.* **2013**, *25*, 6385.
[50] E. B. Luiz, C. C. Juliana, M. Vijayan, L. C. Ana, S. B. Nupura, A. A. Wesleyan, Z. Pinar, E. V. Nihal, M. G. Amir, R. D. Mehmet, K. Ali, *Biofabrication* **2014**, *6*, 024105.
[51] M. Nikkhah, N. Eshak, P. Zorlutuna, N. Annabi, M. Castello, K. Kim, A. Dolatshahi-Pirouz, F. Edalat, H. Bae, Y. Yang, A. Khademhosseini, *Biomaterials* **2012**, *33*, 9009.
[52] H. Shin, B. D. Olsen, A. Khademhosseini, *Biomaterials* **2012**, *33*, 3143.
[53] O. O. P. Hanninen, M. Atalay, *Renal Excretion, Endocrinology, Respiration, Blood Circulation: Its Dynamics and Physiological Control, Physiology and Maintenance*, Volume *III*, EOLSS Publications, Oxford, UK **2009**.
[54] D. Rizzoni, C. Aalkjaer, C. De Ciuceis, E. Porteri, C. Rossini, C. A. Rosei, A. Sarkar, E. A. Rosei, *High Blood Pressure Cardiovasc. Prev.* **2011**, *18*, 169.
[55] J. A. Walocha, J. A. Litwin, T. Bereza, W. Klimek-Piotrowska, A. J. Miodoński, *Hum. Reprod.* **2012**, *27*, 727.
[56] a) C. M. Nelson, R. P. Jean, J. L. Tan, W. F. Liu, N. J. Sniadecki, A. A. Spector, C. S. Chen, *Proc. Natl. Acad. Sci. USA* **2005**, *102*, 11594; b) N. C. Rivron, E. J. Vrij, J. Rouwkema, S. Le Gac, A. van den Berg, R. K. Truckenmüller, C. A. van Blitterswijk, *Proc. Natl. Acad. Sci. USA* **2012**, *109*, 6886.
[57] V. Hosseini, P. Kollmannsberger, S. Ahadian, S. Ostrovidov, H. Kaji, V. Vogel, A. Khademhosseini, *Small* **2014**, *10*, 4851.
[58] Y. C. Chen, R. Z. Lin, H. Qi, Y. Yang, H. Bae, J. M. Melero-Martin, A. Khademhosseini, *Adv. Funct. Mater.* **2012**, *22*, 2027.
[59] N. Huebsch, P. R. Arany, A. S. Mao, D. Shvartsman, O. A. Ali, S. A. Bencherif, J. Rivera-Feliciano, D. J. Mooney, *Nat. Mater.* **2010**, *9*, 518.
[60] C. Cha, S. R. Shin, X. Gao, N. Annabi, M. R. Dokmeci, X. S. Tang, A. Khademhosseini, *Small* **2014**, *10*, 514.
[61] a) A. Suciu, G. Civelekoglu, Y. Tardy, J. J. Meister, *Bull. Math. Biol.* **1997**, *59*, 1029; b) S. Ostrovidov, S. Ahadian, J. Ramon-Azcon, V. Hosseini, T. Fujie, S. P. Parthiban, H. Shiku, T. Matsue, H. Kaji, M. Ramalingam, H. Bae, A. Khademhosseini, *J. Tissue Eng. Regener. Med.* **2014**, *11*, 582.
[62] K. J. Livak, T. D. Schmittgen, *Methods* **2001**, *25*, 402.

